First-principles study of dislocations in hcp metals through the investigation of the $(11\bar{2}1)$ twin boundary

Nina J. Lane,[1,*] Sergei I. Simak,[2] Arkady S. Mikhaylushkin,[2] Igor A. Abrikosov,[2] Lars Hultman,[2] and Michel W. Barsoum[1]

[1]*Department of Materials Science and Engineering, Drexel University, Philadelphia, PA 19104*
[2]*Department of Physics, Chemistry and Biology, Linköping University, SE-581 83 Linköping, Sweden*

Herein, we use first principles calculations to study the energy of the $(11\bar{2}1)$ twin boundary in Zr, Zn, Mg, Ti, and Be. This boundary is important for understanding the microyielding and damping of hexagonal close-packed metals. The $(11\bar{2}1)$ twin boundary is unique in that it is composed of—and can form by the glide of—basal dislocations nucleating at every c lattice parameter. The effect of the number of atoms between boundaries on the boundary energy, and the resulting lattice strains of the relaxed structures are quantified. It is shown that the energies obtained converge within 32–64 atoms/supercell. The structures with a higher second-order elastic constant term, c_{44}, also have higher boundary energies. It is further shown that the critical resolved shear stresses of the basal dislocations at 0 K, which make up the $(11\bar{2}1)$ twin, are so low as to be below the threshold of the first principles calculations.

I. INTRODUCTION

Hexagonal metals (HM) have been studied for decades due to their technological importance. While their mechanisms for plastic deformation under high strains are widely accepted, their low-strain ($\varepsilon < 1\%$) behavior has, until recently, not been very well understood. The deformation of HM under low strains is a crucial piece of the deformation puzzle for HM, especially when considering phenomena such as microyielding and damping. A breakthrough toward understanding the early deformation of HM came about recently when we showed that they are kinking nonlinear elastic (KNE) solids.[1–3] Macroscopically, KNE solids are characterized by the formation of fully, and spontaneously, reversible closed hysteresis stress-strain loops. The size of these loops, which corresponds to the energy dissipated per unit volume, scales with the maximum applied stress squared and is a strong function of grain size.

It is currently postulated that the deformation mechanism that leads to these characteristic stress-strain loops involves the nucleation, growth, and annihilation of incipient kink bands (IKBs).[4] IKBs [Fig. 1(a)] are concentric dislocation loops that nucleate and grow under an applied load, and they are spontaneously annihilated when the load is removed. A sufficient condition for a solid to be KNE is plastic anisotropy, where the dislocations are confined to two dimensions— usually the basal planes in hexagonal metals. Characteristics that often lead to this include a high c/a ratio and low c_{44}, where c and a are the lattice constants of the unit cell, and c_{44} is the second-order elastic shear constant. Most layered solids, graphite, the $M_{n+1}AX_n$ phases, and mica can also be classified as KNE solids, among others.[1,5–7]

Macro- and microscale models for the deformation of KNE solids have been developed and agree well with experimental results.[6,7] However, modeling at the atomic level is still lacking. To fully describe the nucleation and growth of IKBs [Fig. 1(a)], and their transformation to mobile dislocation walls (MDWs) [Fig. 1(a)], and ultimately kink bands (KBs) [Fig. 1(b)], it is essential to understand the structure of the MDWs [Fig. 1(c)].

The ultimate goal of this work is to model IKBs and their nucleation from an atomistic point of view. The goal of this paper, however, is much more modest and represents a first step towards our ultimate goal, in that we chose to study the atomistics of the $(11\bar{2}1)$ twin in HM. The $(11\bar{2}1)$ twin is of particular interest because it is a special kink boundary in which a basal plane dislocation is nucleated every c lattice parameter [Fig. 1(d)]. The $(11\bar{2}1)$ twin stands out as the only twin in which all lattice sites are correctly sheared to their twin positions, and lattice shuffles are thus not required.[8] Said otherwise, this twin can form solely by basal dislocation glide. Study of this twin can be traced back to Palache,[9] who reported the twinning features in graphite as $(11\bar{2}1)$ twins. A full description of the structure of all twinning elements of this boundary was first provided by Freise and Kelly,[10] who identified the $(11\bar{2}1)$ twin boundary as a wall of basal dislocations in graphite. Based on Shockley and Read's model for the energy of dislocations along a grain boundary,[11] they proposed that the $(11\bar{2}1)$ twin was composed of alternating partial dislocations along the boundary. Minonishi *et al.*[12] also found that the stable relaxed structure at the interface leads to a change in stacking sequence across the boundary [see Fig. 2(a) and 2(b)], which renders it effectively shuffleless. Similar results were obtained by Serra and Bacon.[13] Since this kink boundary is, at first approximation, a boundary of edge and screw dislocations, it follows that investigation of the energy and structure of the $(11\bar{2}1)$ twin would be useful for enhancing our understanding of dislocations, KBs, and ultimately KNE solids. To our knowledge, the $(11\bar{2}1)$ twin has to date not been investigated using first principles calculations in the way it is dealt with herein.

Among atomistic modeling approaches, emphasis is put on first principles, or *ab initio*, calculations based on full electronic structures for obtaining accurate energies. However, the study of dislocations is not a well-tested territory for *ab initio* calculations since the supercells needed to adequately account for the long-range elastic fields can be quite large. With a supercell approach, it is difficult to isolate the effects of the dislocations, or defects within the cell, from the surface
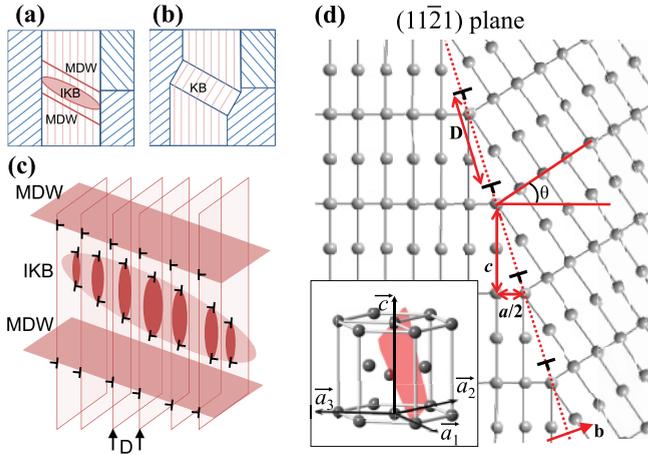
FIG. 1. (Color online) Schematic of (a) an IKB, (b) KBs, and (c) the dislocation structure of the IKB and MDWs shown in (a). The $(1\bar{1}00)$ plane view of the $(11\bar{2}1)$ twin is shown in (d), showing the $(11\bar{2}1)$ plane (dotted line), the twin angle θ, and edge dislocations every c lattice parameter. Inset (bottom left) shows the $(11\bar{2}1)$ plane.

FIG. 2. (Color online) (a) $(1\bar{1}00)$ plane view of relaxed atom positions of repeating structure with two $(11\bar{2}1)$ twin boundaries for a 32 atom, unit cell, showing $(11\bar{2}1)$ planes (red lines) and the boundaries for the unit cell (dotted lines). (b) The structure of the $(11\bar{2}1)$ twin in an hcp material in the $(\bar{1}1\bar{2}6)$ plane projection. (c) $(1\bar{1}00)$ plane projection of the $(11\bar{2}1)$ twin, illustrating stacking sequence. Red line represents the $(11\bar{2}1)$ plane. For (b) and (c), green, yellow, and pink atoms correspond to A, B, and C stacking, respectively (see inset, bottom right); solid and striped atoms correspond to matrix (ABAB) and twin (ACAC) lattice, respectively.

effects caused by its periodicity. To eliminate surface effects, full periodic boundary conditions must therefore be satisfied, which is only possible if the Burgers vector of the supercell is zero. This approach has been employed for dislocation cores in cubic systems[14–16] and boundary surface energies in Mg,[17] but generally the use of *ab initio* calculations to study boundaries and dislocations has still been few and far between. The main reason for this is the computational limitations for the large number of atoms required, along with the boundary conditions, which impose limitations on the special boundary structures that can be simulated.

The purpose of this study is to report on the energy and structure of the $(11\bar{2}1)$ twin in the HMs Mg, Ti, Zn, Zr, and Be, through the supercell approach using *ab initio* calculations. The effects of supercell size on the boundary energies, for each element, are considered. We also calculate the unit cell parameters and c_{44} and explore how these parameters relate to our results on the twin boundary energies. The critical resolved shear stresses of the dislocations are also estimated to be *below* the threshold of the *ab initio* calculations.

II. CALCULATIONS

Ab initio calculations based on density functional theory (DFT) were performed using the projector-augmented wave (PAW)[18,19] method, as implemented in the VASP code.[20–23] The exchange-correlation function used was the Perdew-Burke-Ernzerhof (PBE) generalized gradient approximation (GGA).[24] The potential for Zr included $4s$ semicore states. The boundary energy calculations involved calculating the total energy of twinned and perfect crystal structures, with the same number of atoms per unit cell. For each set of calculations, a supercell of the perfect crystal structure, with the required number of atoms, was used to converge the

k-point mesh and plane wave cutoff with respect to the c/a ratio, compressibility (bulk modulus), and equilibrium volume relaxation. This led to a plane wave cutoff of 210 eV, 178 eV, 276 eV, 230 eV, and 247 eV for Mg, Ti, Zn, Zr, and Be, respectively, and Γ-centered k-point grids of $25 \times 25 \times 25$ for 2 atoms, $9 \times 9 \times 9$ for 32 atoms, and $5 \times 5 \times 5$ for 64 and 80 atoms. For each structure, the total energy was converged to 10^{-6} eV/cell at fixed volumes while relaxing the c/a ratio and atomic positions. The equilibrium structure and energy were determined by fitting the total energy as a function of volume to the modified Morse equation of state.[25]

For the twin boundary calculations, supercells with two $(11\bar{2}1)$ twin boundaries consisting of 32, 64, and 80 atoms were constructed. This was accomplished by shifting the hexagonal coordinates to orthogonal axes, with the x direction normal to the $(11\bar{2}1)$ plane and the y and z directions parallel to the plane. Figure 2(a) shows a unit cell with 32 atoms, consisting of rows of undistorted hexagonal close-packed (hcp) crystals with 7 atomic planes between the boundaries. Supercells with 64 and 80 atoms (not shown) consist of 15 and 20 atomic planes, respectively, between the boundaries. After slicing the cell along the $(11\bar{2}1)$ plane and mirroring the structure about the plane, a shift from ABAB to ACAC stacking sequence across the boundary is necessary, resulting in the structures shown in Fig. 2(b) and (c).

TABLE I. Interfacial energies and angles of the $(11\bar{2}1)$ twin boundary in selected hcp metals for different supercell sizes, compared to values obtained in previous work.

Metal	Supercell size	Interfacial energy (mJ/m^2)		θ (degrees)
		This work	Previous work	
Mg	32	122.3	147[a],480[b]	31.7
	64	127.3		
	80	125.6		
Ti	32	238.0	150[a], 180.8[c]	32.4
	64	234.9		
	80	233.2		
Zr	32	235.1	169[a]	32.0
	64	228.7		
Zn	32	230.7	480[b]	27.5
	64	196.3		
Be	32	1034.4	1810[b]	32.4
	64	1073.3		

[a]From Reference 27, Finnis–Sinclair (FS) embedded-atom potential technique.
[b]From Reference 28, based on pseudopotential theory.
[c]From Reference 12, from Lennard-Jones potential fitted to Ti truncated between sixth and seventh nearest neighbors.

The boundary interfacial energy, $E_{(11\bar{2}1)}$, was extracted from the energy of the supercell and the energy of a perfect hcp crystal, assuming,

$$E_{(11\bar{2}1)} = \frac{n(E_{\text{supercell}} - E_{\text{hcp}})}{2 \cdot A}, \qquad (1)$$

where n is the number of atoms in the supercell, and $E_{\text{supercell}}$ and E_{hcp} are the energies per atom of the supercell with the twin boundary and the perfect hcp crystal, respectively. A is the area of the boundary given by the cross product of the axes in the x and z directions.

As noted already, and for reasons discussed later herein, our analysis also involves c_{44}. This was calculated by applying lattice distortions and deriving the elastic constants from the stress-strain relationship,[26] as implemented in VASP 5.2.

III. RESULTS AND DISCUSSION

The results of the interfacial energy calculations on the $(11\bar{2}1)$ boundary are summarized in Table I, along with values previously calculated using other methods[12,27,28] and the twin boundary θ. With the exception of Zn, increasing the number of atoms to 64 atoms only changes the energy of the boundary by less than 5% compared to 32 atoms. The larger differences for Zn are most likely due to the distortion from ideal packing indicated by the anomalously large c/a structure. In general, however, the fact that the boundary energy contribution to the total cell energy does not change significantly with the number of atoms implies that there is no considerable interaction between the boundaries, and thus the dislocations along them, at these supercell sizes. Therefore, for most of the hcp metals studied herein, the small number of atoms was considered sufficient for the purposes of calculating boundary/dislocation structures.

Since there are no previous *ab initio* calculations on the $(11\bar{2}1)$ boundary for comparison, we can only judge the values obtained against other techniques, such as the embedded atom method (EAM)[29] and Finnis-Sinclair (FS)[30] method. Both of these are considered less accurate than *ab initio* calculations, especially for materials where covalent bonding is important, such as Ti, Zr, or, especially, Be. Previous work on hcp twins has shown that while structures produced by empirical models are fairly close to those obtained from *ab initio* calculations, the energies can be quite different.[31] Generally, EAM and FS methods lead to a wide range of energy values that vary significantly in either direction, demonstrating the need for accurate potentials. For example, in Zr, the $(10\bar{1}2)$ twin, which is morphologically similar to the $(11\bar{2}1)$ twin, yields a boundary energy of 150 mJ/m^2 [32] and 151 mJ/m^2 [33] from *ab initio* studies, while the results from FS simulations lead to 262 mJ/m^2 [31] and 123 mJ/m^2.[33] For the same twin in Mg, *ab initio* calculations lead to a boundary energy of 114 mJ/m^2[31,33] and 118 mJ/m^2,[17] while the results from FS simulations lead to 188 mJ/m^2,[27] and EAM results lead to 800–1010 mJ/m^2.[28]

A more useful evaluation of our results comes from an assessment of them in relation to c_{44}. It is well established in classical dislocation theory that the energy of a dislocation, its core, and the Peierls stress all scale with the shear modulus, G.[11] It is therefore reasonable to assume that the $(11\bar{2}1)$ boundary energy should scale with c_{44}. As a benchmark for evaluating the relative values, our results—as calculated from VASP as outlined in Sec. 1—are listed in Table II. Values also listed in Table II are the ground state parameters for the crystal structures of all HM studied herein, compared with experimental values. All values for the lattice parameters are within 2% of the experimental values, and the bulk moduli are within 6% of the experimental values, lending credibility to the potentials used.

Figure 3 shows that a correlation between the boundary energy and c_{44} indeed exists, with a linear fit having $R^2 = 0.99$. This result is taken as indirect evidence for the validity of our methodology. It is significant to note that the twin boundary energy of Be is approximately an order of magnitude

TABLE II. Calculated lattice parameters, bulk moduli, B, and c_{44} values for HM.

Metal		a (Å)	c (Å)	c/a	B (GPa)	c_{44} (GPa)
Mg	Calc.	3.198	5.174	1.618	37	17.9
	Calc.[a]	3.138	5.107	1.627	37	17.7
	Exp.[b]	3.209	5.211	1.624	36	16.4
Ti	Calc.	2.926	4.612	1.576	116	40.6
	Calc.[a]	2.900	4.671	1.611	123	50.4
	Exp.[b]	2.951	4.684	1.587	110	46.7
Zr	Calc.	3.236	5.171	1.598	96	26.0
	Calc.[a]	3.229	5.166	1.600	101	43.0
	Exp.[b]	3.232	5.148	1.593	97	32.1
Zn	Calc.	2.643	5.087	1.925	58	38.8
	Calc.[d,e]	2.648	5.085	1.921	60	23.2
	Exp.[b]	2.665	4.947	1.856	60	39.6
Be	Calc.	2.264	3.573	1.578	122	159.7
	Calc.[c]	2.294	3.608	1.573	122	160.2
	Exp.[b]	2.287	3.583	1.567	114	162.5

[a]From Reference 60.
[b]From Reference 61.
[c]From Reference 62.
[d]From Reference 63.
[e]From Reference 64 for c_{44}.

higher than the other metals studied. Its bulk modulus and total energies, however, are *comparable* to Ti, and thus the higher boundary energy of Be cannot be related to its compressibility or be an artifact of the energy relaxations. The fact that c_{44} of Be is also about an order of magnitude higher than the other metals studied is thus significant and consistent with the notion that the boundary energy is related to the energy of the dislocations.

The way dislocations move is contingent on the energetics of bonding related to the dislocation core. As a loose definition, one can define the core as the region of crystal lattice around the dislocation line in which the relative displacement of the
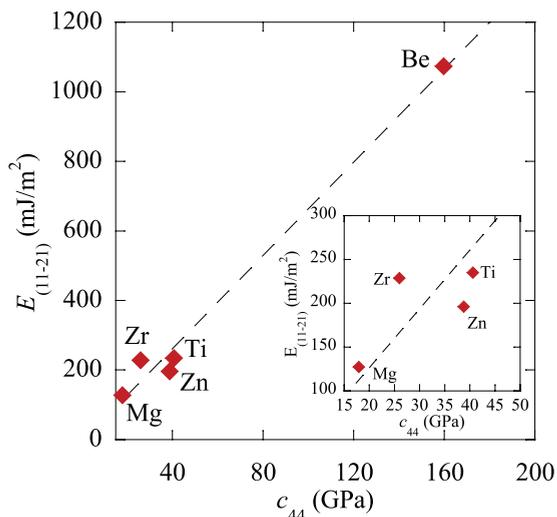
FIG. 3. (Color online) Twin boundary energy vs c_{44} calculated for Ti, Zr, Zn, Mg, and Be. Inset shows plot zoomed into lower-left region. Least squares fit of the results yields a correlation coefficient, R^2, of 0.99.

neighboring atoms exceeds the elastic limit (for example, 2% in terms of local shear strain).[34] Because core structure, under zero stress, has been given importance for its connection to mechanisms of dislocation motion,[31,35–38] the equilibrium structure of the bonding in and around the boundary should be considered as well. Figure 4 shows the variations of inter-atomic distances within the basal planes in the 80 atom ($11\bar{2}1$) supercell of Mg, as compared to the equilibrium structure obtained herein (Table II). All atomistic configurations are visualized using Atomeye software.[39] Consistent with the limited effect of the number of atoms on the boundary energies, the size of the distorted regions is similar for all supercell sizes studied.

Figure 5 shows the von Mises shear strain invariant, which is a way of representing the strain fields of each atomic environment compared to the system average, or the overall local distortion as compared to the perfect crystal, as implemented in Atomeye.[40] Here again, the von Mises strains on the atoms away from the boundary are close to zero. Along the basal planes, the absolute effective "strain" falls below 1.5% at a distance of approximately $1.5a$ from the boundary. Similar results (not shown) were obtained for the other elements explored herein, regardless of their boundary energies. Because the relative displacements of the atoms outside of the strained regions, or effective core, do not contribute much to the energy of dislocation transla-tion, the small deviation in the core size implies that for solids with higher boundary energies, such as Be, the bond stretching and bending involved are much more energetically expensive.

We can go further in our assessment of the mobility of this boundary by not only identifying the regions where atom distances deviate from equilibrium, but also by assessing the dislocation structure within this region. As noted already, not only is the structure of the ($11\bar{2}1$) twin composed of dislocations, but the latter are glissile. Freise and Kelly[10] and Minonishi *et al.*[12] found that the stable relaxed structure at the interface leads to a change in stacking sequence across the boundary [see Figs. 2(a) and 2(b)], which enables the boundary to *move*, within the basal planes, with effectively no atomic rearrangements. We note in passing that the work of Serra and Bacon,[13] on the same boundary, is so different from our approach that no meaningful comparisons can be made. For example, they identified the twin dislocations as being mixed with edge and screw components in the ($11\bar{2}6$) direction and pointed out that despite the small magnitude of the Burgers vector, $\sim a/7$, the core registry is spread over a region 50–100 times this in width, suggesting that the step may be very mobile.[41] Herein, we treat the boundary as a low-angle grain boundary with a Burgers vector equal to a.

Experimentally, the mechanical damping effect due to reversible ($11\bar{2}1$) twin boundary movement was found in Zr[42–44] as well as Co,[45] which is also consistent with the fact that dislocations along the ($11\bar{2}1$) twin are mobile and result in reversible crystal slipping on a single glide. To investigate this further, we explored the atomic shifts and energies involved in shifting the boundary by a Burgers vector along the basal planes in 32 atom supercells [Fig. 6]. The structures with the original [Fig. 6(a)] and shifted [Fig. 6(b)] boundaries were
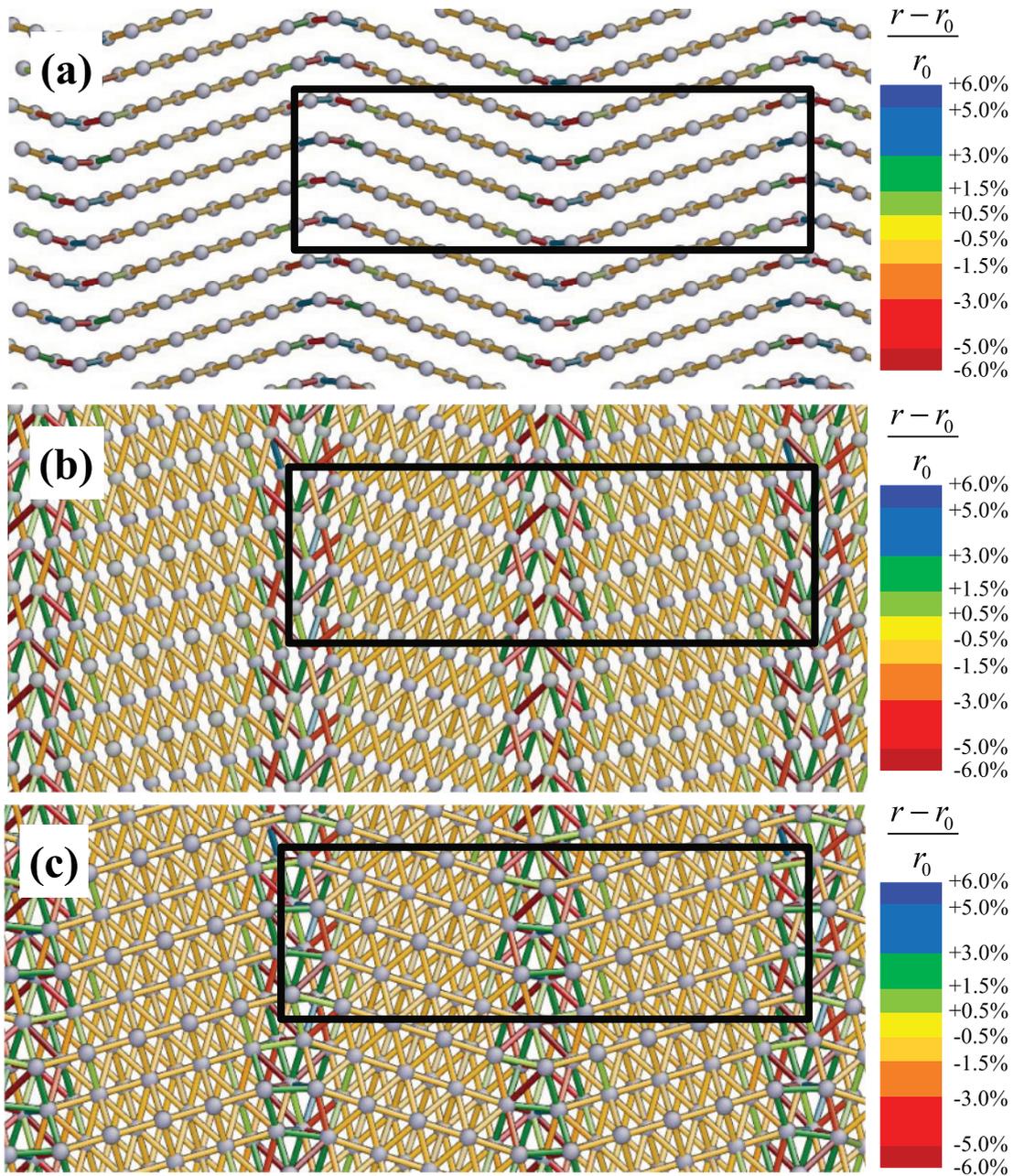
FIG. 4. (Color online) Relative interatomic distances of structure obtained from the *ab initio* energy relaxations of the $(11\bar{2}1)$ twin supercell for Mg with 80 atoms. Deviations of interatomic distances are represented as strains compared to r_0, the interatomic distances in the unit cell from *ab initio* calculations. For clarity, (a) shows only strains along the *a* direction, (b) shows only strains in the *c* direction, and (c) shows interatomic distances between all nearest neighbors. Boundary of repeating supercell is shown as dark rectangle.

first relaxed as described in Sec. II, and a chain of seven images was generated by linear interpolation between the two end structures. We used the nudged elastic band method,[46,47] as implemented by VASP, to simultaneously optimize the intermediate images and calculate the energy barrier to move the atoms into the atomic positions of the shifted boundary. For both Mg and Be, the energy is extremely small; at <0.1 mJ/m^2, the difference in boundary energy as a barrier is below the resolution of the *ab initio* calculations, indicating that factors beyond detection of modeling at the atomic scale

must be dominant for dislocation glide. As far as we are aware, this is the first time such a conclusion has been reached using *ab initio* calculations for basal plane dislocations in HM. This conclusion is in agreement with the fact that Tinder and Washburn[48] were unable to measure a threshold stress for the motion of dislocations in pure Cu. They also clearly showed that plastic deformation commences from almost zero stress in copper and zinc.[49] These findings are also in line with the results reported by Roberts and Brown[50,51] for zinc and the results of Brydges,[52] who later showed that the critical resolved
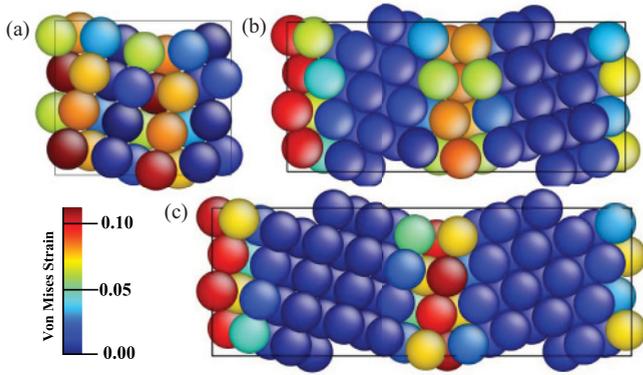
FIG. 5. (Color online) Von Mises shear strain maps of atomistic configurations from relaxed $(11\bar{2}1)$ twin structures with repeating unit cells containing (a) 32 atoms, (b) 64 atoms, and (c) 80 atoms.

shear stress (CRSS) in pure Cu single crystals continuously decreased with decreasing dislocation density.

This work on Zn and Cu is also consistent with results by Roberts and Hartman[53,54] on Mg. In 1964, they published a paper on the temperature dependence of microyielding stresses in Mg single crystals.[54] In that work, they reported that at shear stresses, τ higher than about 0.04 to 0.07 MPa, fully and spontaneously reversible, closed stress-strain loops were observed. At about 0.35 MPa, the loops were no longer closed. In Fig. 3 of their paper, they published the loops for one of their samples—tested at room temperature—that was pre-deformed to a shear strain of 0.66% prior to cycling. More importantly, they noted that initial loading of annealed samples to *any* stress level always resulted in permanent strain. In other words, the yield point for as-received samples was below the detectability limit of their equipment, i.e., < 0.01 MPa. Recently, we showed that damping and microyielding in Mg were due to the nucleation and growth of IKBs.[55,56] When we apply our IKB model to their results, we obtain CRSS values of the order of 0.02 MPa for the crystals that were pre-deformed to 0.66%.

As noted by Agnew and Nie in a recent review of Mg,[57] it is still not known what exactly dictates the nucleation and growth of twins nor what dictates the CRSS. Hutchinson and Barnett[58] have also emphasized the disparate nature of the data for CRSS from tensile or compressive testing of single crystals, and the fact that the CRSS values used for polycrystal modeling have a much narrower distribution. For hcp metals, it is likely that the mobility of dislocation walls is dictated by extrinsic barriers such as other dislocations, defects, or precipitates, which would also explain the disparate nature of CRSS when grain boundaries are introduced (i.e., for polycrystalline materials). However, given the fact that dislocation glide is generally observed as the easiest system for accommodating stresses[59] and that the $(11\bar{2}1)$ twin has been observed to be mobile,[11,27,41] as confirmed herein, these results are consistent with the IKB model when considering the ability of dislocations to move reversibly at the atomic scale. Directions for future calculations in analyzing the full reversible motion of dislocation walls lie in identifying the extrinsic factors, perhaps at other length scales, that may play a role during IKB formation and annihilation.

Overall, the results on the convergence of energy with supercell size show us that the difference in total energy is indeed introduced by the boundaries and not the atoms in between them, nor the interactions between boundaries. Furthermore, the energy convergence with supercell size indicates that the smallest number of atoms (i.e., 32) is, for these materials, sufficient for investigating the energy effects of the dislocation structures. Thus, this is a sound method for calculating the energy induced by dislocations without having to go to extremely large numbers of atoms.

IV. CONCLUSIONS

The energy and atom arrangements of the $(11\bar{2}1)$ twin boundary in Mg, Ti, Zr, Zn, and Be were determined from *ab initio* calculations. The boundary energies scale linearly with c_{44}. The dislocation energy and core structure for the supercell with 32 atoms are sufficient and provide similar results as the supercell with 80 atoms. The study of the core arrangement and energetics of the $(11\bar{2}1)$ boundary through *ab initio* methods can shed light onto the dislocation motion through basal slip, and thus the deformation of hcp solids through kinking.

FIG. 6. (Color online) Illustration of the movement of the dislocation boundaries (dashed lines) by one Burgers vector: (a) initial positions and (b) positions after the boundary has shifted one Burgers vector, shown by the red arrow. Original atom positions are also shown by the hatched circles to illustrate the movement of individual atoms.

*Corresponding author: lane@drexel.edu

[1] A. G. Zhou, S. Basu, and M. W. Barsoum, Acta Mater. **56**, 60 (2008).

[2] A. Zhou and M. Barsoum, Metall. Mater. Trans. A **40**, 1741 (2009).

[3] A. G. Zhou, D. Brown, S. Vogel, O. Yeheskel, and M. W. Barsoum, Mater. Sci. Eng. A **527**, 4664 (2010).

[4] M. W. Barsoum and S. Basu, in *Encyclopedia of Materials: Science and Technology*, edited by J. Buschow, R. Cahn, M. C. Flemings, B. Ilschner, E. J. Kramer, S. Mahajan, and P. Veyssiere (Elsevier, Oxford, 2010), p. 1.

[5] M. W. Barsoum, A. Murugaiah, S. R. Kalidindi, and T. Zhen, Phys. Rev. Lett. **92**, 255508 (2004).

[6] M. W. Barsoum, T. Zhen, A. Zhou, S. Basu, and S. R. Kalidindi, Phys. Rev. B **71**, 134101 (2005).

[7] S. R. Kalidindi, T. Zhen, and M. W. Barsoum, Mater. Sci. Eng. A **418**, 95 (2006).

[8] J. W. Christian and S. Mahajan, Prog. Mater. Sci. **39**, 1 (1995).

[9] C. Palache, Am. Mineral. **26**, 709 (1941).

[10] E. J. Freise and A. Kelly, Proc. Phys. Soc. A **264**, 269 (1961).

[11] W. T. Read and W. Shockley, Phys. Rev. **78**, 275 (1950).

[12] Y. Minonishi, S. Ishioka, M. Koiwa, and S. Morozumi, Phys. Status Sol. A **71**, 253 (1982).

[13] A. Serra and D. J. Bacon, Philos. Mag. A **54**, 793 (1986).

[14] A. Arya and E. A. Carter, J. Chem. Phys. **118**, 8982 (2003).

[15] E. Clouet, L. Ventelon, and F. Willaime, Phys. Rev. Lett. **102**, 055502 (2009).

[16] L. Ventelon and F. Willaime, J. Comput.-Aided Mol. Des. **14**, 85 (2008).

[17] Y. Wang, L. Q. Chen, Z. K. Liu, and S. N. Mathaudhu, Scr. Mater. **62**, 646 (2010).

[18] P. E. Blochl, Phys. Rev. B **50**, 17953 (1994).

[19] G. Kresse and D. Joubert, Phys. Rev. B **59**, 1758 (1999).

[20] G. Kresse and J. Hafner, Phys. Rev. B **47**, 558 (1993).

[21] G. Kresse, and J. Hafner, Phys. Rev. B **49**, 14251 (1994).

[22] G. Kresse and J. Furthmuller, Phys. Rev. B **54**, 11169 (1996).

[23] G. Kresse and J. Furthmuller, Comp. Mater. Sci. **6**, 15 (1996).

[24] J. P. Perdew, K. Burke, and M. Ernzerhof, Phys. Rev. Lett. **77**, 3865 (1996).

[25] V. L. Moruzzi, J. F. Janak, and K. Schwarz, Phys. Rev. B **37**, 790 (1988).

[26] Y. Le Page and P. Saxe, Phys. Rev. B **65**, 104104 (2002).

[27] A. Serra and D. J. Bacon, Philos. Mag. A **63**, 1001 (1991).

[28] J. P. Simon, J. Phys. F, Met. Phys. **10**, 337 (1980).

[29] M. S. Daw and M. I. Baskes, Phys. Rev. B **29**, 6443 (1984).

[30] M. W. Finnis and J. E. Sinclair, Philos. Mag. A **50**, 45 (1984).

[31] M. H. Yoo, J. R. Morris, K. M. Ho, and S. R. Agnew, Metall. Mater. Trans. A **33**, 813 (2002).

[32] J. R. Morris, Y. Y. Ye, K. M. Ho, C. T. Chan, and M. H. Yoo, Philos. Mag. A **72**, 751 (1995).

[33] J. R. Morris, Y. Y. Ye, and M. H. Yoo, Philos. Mag. **85**, 233 (2005).

[34] W. Cai, V. V. Bulatov, J. Chang, J. Li, and S. Yip, in *Dislocations in Solids*, edited by F. R. N. Nabarro and J. P. Hirth (Elsevier, North-Holland, 2004), Vol. 12.

[35] V. Vitek, Philos. Mag. **84**, 415 (2004).

[36] V. Vitek and M. Igarashi, Philos. Mag. A **63**, 1059 (1991).

[37] V. Vitek, Trans. Indian Inst. Met. **38**, 510 (1985).

[38] J. A. Yasi, T. Nogaret, D. R. Trinkle, Y. Qi, L. G. Hector, and W. A. Curtin, Modell. Simul. Mater. Sci. Eng. **17**, 055012 (2009).

[39] J. Li, Modell. Simul. Mater. Sci. Eng. **11**, 173 (2003).

[40] J. Li, Ph.D. thesis, Massachusetts Institute of Technology, 2000.

[41] A. Serra, D. J. Bacon, and R. C. Pond, Acta Metall. **36**, 3183 (1988).

[42] R. E. Reed-Hill, E. P. Dahlberg, and W. A. J. Slippy, Trans. Met. Soc. AIME **223**, 1766 (1965).

[43] A. Akhtar and A. Teghtsoonian, Acta Metall. **19**, 655 (1971).

[44] J. F. Bingert, T. A. Mason, G. C. Kaschner, P. J. Maudlin, and G. T. Gray, Metall. Mater. Trans. A **33**, 955 (2002).

[45] S. Vaidya and S. Mahajan, Acta Metall. **28**, 1123 (1980).

[46] G. Mills, H. Jónsson, and G. K. Schenter, Surf. Sci. **324**, 305 (1995).

[47] H. Jónsson, G. Mills, and K. W. Jacobsen, in *Classical and Quantum Dynamics in Condensed Phase Simulations*, edited by B. J. Berne, G. Ciccotti, and D. F. Coker (World Scientific, Singapore, 1998), p. 385.

[48] R. F. Tinder and J. Washburn, Acta Metall. **12**, 129 (1964).

[49] R. F. Tinder and J. Washburn, 22nd Technical Report, UC Berkeley California Part I, Minerals Res. Lab (UC California, Berkeley, 1962).

[50] J. M. Roberts and N. Brown, Trans. AIME **218**, 454 (1960).

[51] J. M. Roberts and N. Brown, Acta. Metall. **10**, 430 (1962).

[52] W. T. Brydges, Philos. Mag. **15**, 1079 (1967).

[53] J. M. Roberts and D. E. Hartman, J. Phys. Soc. Jpn. **18**, 119 (1963).

[54] J. M. Roberts and D. E. Hartman, Trans. AIME **230**, 1125 (1964).

[55] A. G. Zhou, B. Basu, and M. W. Barsoum, Acta Mater. **56**, 60 (2008).

[56] A. Zhou and M. W. Barsoum, Metall. Mater. Trans. **40A**, 1741 (2009).

[57] S. R. Agnew and J. F. Nie, Scr. Mater. **63**, 671 (2010).

[58] W. B. Hutchinson and M. R. Barnett, Scr. Mater. **63**, 737 (2010).

[59] J. J. Jonas, S. Mu, T. Al-Samman, G. Gottstein, L. Jiang, and T. Martin, Acta Mater. **59**, 2046 (2011).

[60] Y. Nie and Y. Xie, Phys. Rev. B **75**, 174117 (2007).

[61] P. Eckerline and H. Kandler, Eds., *Structure Data of Elements and Intermetallic Phases* (Springer-Verlag, New York, 1971).

[62] G. Sin'ko and N. Smirnov, Phys. Rev. B **71**, 214108 (2005).

[63] G. Ghosh, S. Delsante, G. Borzone, M. Asta, and R. Ferro, Acta Mater. **54**, 4977 (2006).

[64] S. L. Shang, A. Saengdeejing, Z. G. Mei, D. E. Kim, H. Zhang, S. Ganeshan, Y. Wang, and Z. K. Liu, Comp. Mater. Sci. **48**, 813 (2010).